Hindawi
Advances in Civil Engineering
Volume 2019, Article ID 5239374, 11 pages
https://doi.org/10.1155/2019/5239374

Research Article

Effect of the Confining Pressure on the Dynamic Compression Properties of Transversely Isotropic Rocks

Xuefeng Ou,[1,2] **Xuemin Zhang**,[2,3] **Han Feng**,[2] **Cong Zhang**,[2] **and Junsheng Yang**[2]

[1]*School of Civil Engineering, Changsha University of Science & Technology, Changsha, Hunan, China*
[2]*School of Civil Engineering, Central South University, Changsha, Hunan, China*
[3]*The Key Laboratory of Engineering Structures of Heavy Haul Railway, Central South University, Changsha, China*

Correspondence should be addressed to Xuemin Zhang; zhangxm@csu.edu.cn

Received 20 September 2018; Accepted 10 March 2019; Published 1 April 2019

Guest Editor: Jian Sun

The dynamic compression properties of transversely isotropic rocks and their dependence on the confining pressure and bedding directivity are important in deep underground engineering activities. In this study, a slate is characterized using a split Hopkinson pressure bar (SHPB) test. Five groups of samples with preferred bedding directions (dip angles of 0°, 30°, 45°, 60°, and 90°) are subjected to coupled axial impact loading (low, medium, and high) under confining pressure (0, 5, and 10 MPa). The failure mode, dynamic strength, and Young's modulus are investigated. The test results show that the tensile splitting effect is significant when there is no confining pressure. However, under a confining pressure (5 and 10 MPa) condition, the cracks that develop along the loading direction can be significantly constrained and the samples are forced to fail along the bedding plane. With increasing confining pressure, the critical dynamic strength significantly increases, and Young's modulus increases when $\theta \geq 45^\circ$ while it decreases when $\theta \leq 30^\circ$.

1. Introduction

Transversely isotropic rocks, which are widely distributed on the surface of the earth, are a specific form of anisotropic rock. Differ from the isotropic rock has identical properties in all directions, the properties of transversely isotropic rocks vary as the bedding plane direction changes (i.e., the rock contains one dominant direction of planar anisotropy) [1]. This description generally applies to the intact laminated, stratified, bedded sedimentary class, and certain intact foliated metamorphic rocks (e.g., slates, shales, sandstone, and coal) [2, 3].

Over the past several decades, numerous tests, numerical simulations, and analytical calculations on failure modes and mechanical properties have been completed [4–7]. The fracture behaviour under triaxial pressure has been found to differ from that under uniaxial pressure [8]. As the confining pressure is increased, the anisotropic rocks become more ductile [9]. However, most of the previous research has focused on the static state of stress. Many engineering applications, such as blasting and drilling, expose rocks to dynamic loading, potentially inducing underground engineering accidents such as collapse, roof fall, rock burst, and gush events. Therefore, understanding the properties of rocks under dynamic loading is important for engineers to optimize design and construction.

Recently, the dynamic property of anisotropy has received major attention. Dai et al. [10] and Liu et al. [11] studied the dynamic properties of Barre granite with respect to the three principle directions. Qiu et al. used static and dynamic uniaxial compression tests on coal rock to characterize the bedding directivity [12]. Li et al. studied the dynamic tensile properties of phyllite with five dip angles (0°, 30°, 45°, 60°, and 90°) [13]. Koerber et al. described recent advances in the SHPB, namely, by using an image-based approach to investigate polymer-based composite materials [14]. These studies focused primarily on uniaxial impact compression tests. In general, the impact splitting effect is easily detectable in one-dimensional impact tests [15]. However, the test results may not fully characterize the actual properties of the rocks, particularly at deep depths.

In natural conditions, the rock properties are affected by the state of *in situ* stress in the strata before blasting and

boring. Multiple blasting engineering observations and laboratory experiments have indicated that properties such as transmission of the impact wave and the effect of blasting and rock fragmentation differ between triaxial and uniaxial pressure [16]. The confining pressure is generally used in dynamic tests to simulate the *in situ* stress. Christensen et al. [16] was the first to test rock with confining pressure and dynamic loading [17]. Then, the triaxial split Hopkinson pressure bar (SHPB) test system for rocks was quickly implemented worldwide [18]. However, despite its importance, relevant research on transversely isotropic rocks is still relatively scarce.

In this study, we aim to investigate the effect of confining pressure on the failure mode and dynamic compression properties of transversely isotropic rocks. The bedding directivity is also of interest; therefore, five groups of samples ($\theta = 0^\circ$, 30°, 45°, 60°, and 90°) were tested using an SHPB at three load levels (low, medium, and high) and three confining pressures (0 MPa, 5 MPa, and 10 MPa). Testing was conducted with 0 MPa confining pressure for the dynamic uniaxial compression test. Then, the results were analysed to determine how the confining pressure affects the physical properties of the rock samples.

2. Experimental Configuration

2.1. Dynamic Testing Facilities. The SHPB is widely employed for characterizing the dynamic response of rocks [19–22]. This apparatus can achieve a strain rate of 10^1–$10^4\ s^{-1}$, which can match typical dynamic loads associated with rock fragmentation. As shown in Figure 1, a dynamic test was conducted using a 50 mm SHPB system at the Central South University (Hunan, China). A cone-shaped striker was used to generate a half-sine incident wave and provided a constant strain rate to the point of sample failure [23, 24]. This method is suitable for testing rock-like materials. The confining pressure device shown in Figure 2 consists of a steel frame with an associated oil cylinder, a rubber sleeve, and oil inlet/outlet valves. The confining pressure is provided by the oil pressure in the chamber (as pressurized by hand pumping). The confining pressure can reach 200 MPa if necessary.

Based on the one-dimensional stress wave theory [25] and the assumption that stress equilibrium is achieved during dynamic loading (i.e. $\varepsilon_i + \varepsilon_r = \varepsilon_t$), the commonly used formulas for calculating strain rate $\dot{\varepsilon}(t)$, strain $\varepsilon(t)$, and stress $\sigma(t)$ are as follows:

$$\begin{cases} \dot{\varepsilon}(t) = -\dfrac{2C}{l_0}\varepsilon_r, \\ \varepsilon(t) = -\dfrac{2C}{l_0}\displaystyle\int_0^t \varepsilon_r dt, \\ \sigma(t) = \dfrac{A}{A_0}E\varepsilon_t, \end{cases} \tag{1}$$

where C is the P-wave velocity of the bars, E is Young's modulus of the bars, and l_0 is the length of the sample, A and A_0 are the cross-sectional areas of the bars and samples, respectively. The indexing i, r, and t refer to incident, reflected, and transmitted, respectively.

2.2. Dynamic Testing Scheme. The critical failure of the samples at different dip angles is measured using a method that uses high-to-low loading steps to test the samples. The assessment standard is based on rock rupture and debris peeling. Then, the loading of critical failure is defined as the low loading level. Three different loading level (low, medium, and high) are used to test samples of five groups. During the test, the loading level is dependent on the barometric value in the launcher. The barometric values at various confining pressures are shown in Table 1.

2.3. Sample Preparation. Five groups of different bedding dip angles (0°, 30°, 45°, 60°, and 90°) were included in this study. The dynamic test samples were prepared at a slenderness ratio of 0.5 (50 mm diameter and 25 mm length), as shown in Figure 3. To ensure that at least 3 results could be obtained per loading level and confining pressure, 150 rock samples were prepared at five dip angles.

3. Geological and Mechanical Characteristics of the Slate

The studied slate was from Jiangxi Province, China. A chemical composition analysis of the slate yielded the following composition: 59.05% SiO_2, 18.56% Al_2O_3, 6.87% Fe_2O_3, 0.24% CaO, 1.84% MgO, 3.47% K_2O, and 2.03% Na_2O. The microscopic structure has been observed by a scanning electron microscope (SEM). As shown in Figure 4, two major layers exist within this slate, which are the stiffer layer and softer layer, respectively. The stiffer layer mainly contains the schistose structure and close arrangement. The crack is undeveloped in this layer. On the contrary, the softer layer is relatively fragmentized and the crack is significantly developed in this layer. The uniaxial compressive strength (σ_{bc}) and Young's modulus (E) are listed in Table 2.

4. Test Results and Discussion

4.1. Dynamic Equilibrium and Strain Rate. Figure 5 shows a typical result: here, specimen 60-1 is subjected to 5 MPa confining pressure. To apply the cone-shaped striker as intended, the constant strain rate loading is applied until sample failure. Figure 6 shows that the sum of incident stress and the reflected stress waves are almost equal to the transmitted strain wave, which indicates that the force balance on both ends of the sample is maintained during all of the dynamic tests, including those on samples subjected to confining pressure.

4.2. Failure Modes. Firstly, the failure mode of the slate samples at the low loading level is analysed. Figure 7 shows failure patterns of the samples with different bedding angles at the low loading level and three different confining

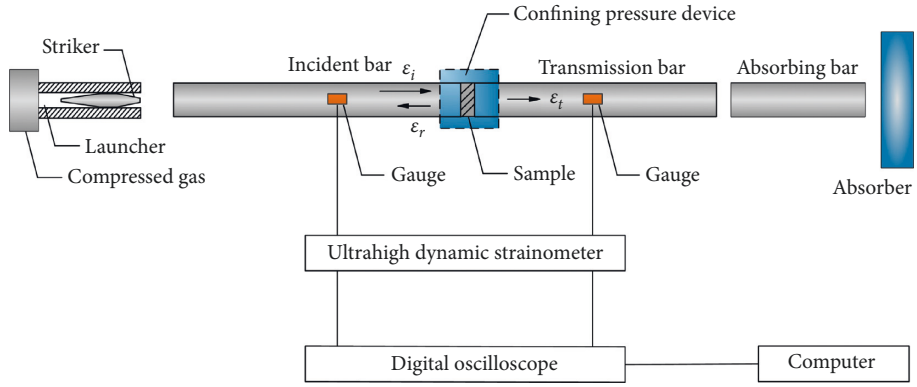

Figure 1: SHPB system with confining pressure device.

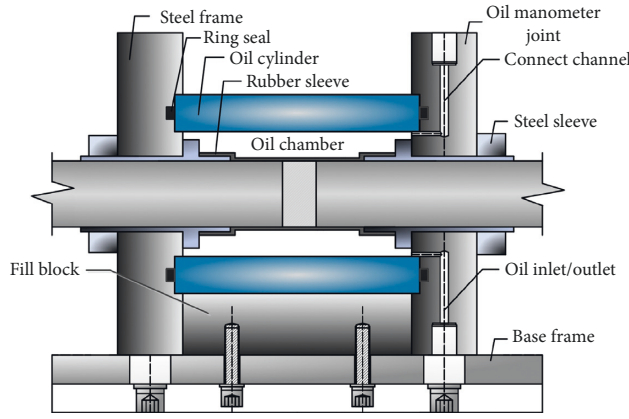

Figure 2: Confining pressure device.

Table 1: Barometric values at various confining pressures and dip angles.

θ	Barometric value (MPa)								
	0 MPa			5 MPa			10 MPa		
	Low	Medium	High	Low	Medium	High	Low	Medium	High
0°	0.7	0.9	1.1	1.0	1.3	1.6	1.4	1.5	1.6
30°	0.4	0.5	0.6	0.6	0.8	0.9	0.9	1.0	1.1
45°	0.3	0.4	0.5	0.4	0.5	0.6	0.5	0.7	0.9
60°	0.3	0.4	0.5	0.5	0.7	0.9	0.5	0.7	0.9
90°	0.3	0.4	0.5	1.0	1.2	1.3	1.0	1.2	1.4

pressures. Four typical failure modes with different dip angles under three different confining pressure can be summarized as follows: (I) tensile splitting across the bedding, (II) shear sliding across the bedding, (III) slide failure along the bedding, and (IV) tensile splitting along the bedding.

Table 3 lists the critical failure modes of the slate samples under different confining pressures. The failure modes of the slate at different confining pressures are similar at $\theta = 0°$, 45°, 60°, and 90°. However, at $\theta = 30°$, the failure mode changes from II to III with the increases of the confining pressure. The difference may result from the confining pressure constraining the development of fractures along the loading direction. In addition, due to the small angle intersection of bedding plane and confining pressure direction, the confining pressure may open the microfractures inherent the bedding planes. Thus, cracks may be prior to develop along the bedding planes.

Figure 8 presents the failure mode of $\theta = 45°$ at high loading level under confining pressure 0 MPa and 10 MPa. When the confining pressure is 0 MPa, the failure pattern of the $\theta = 45°$ sample transitions from a single failure mode (III) to a mixed mode (III + I) with the loading level changes from low to high [25]. However, when the confining pressure is 10 MPa, although many fine cracks develop along the loading direction, the mainly failure mode is still sliding along the bedding plane. It may because the confining pressure can effectively weaken the impact splitting effect and constrain the cracks develop along the loading direction.

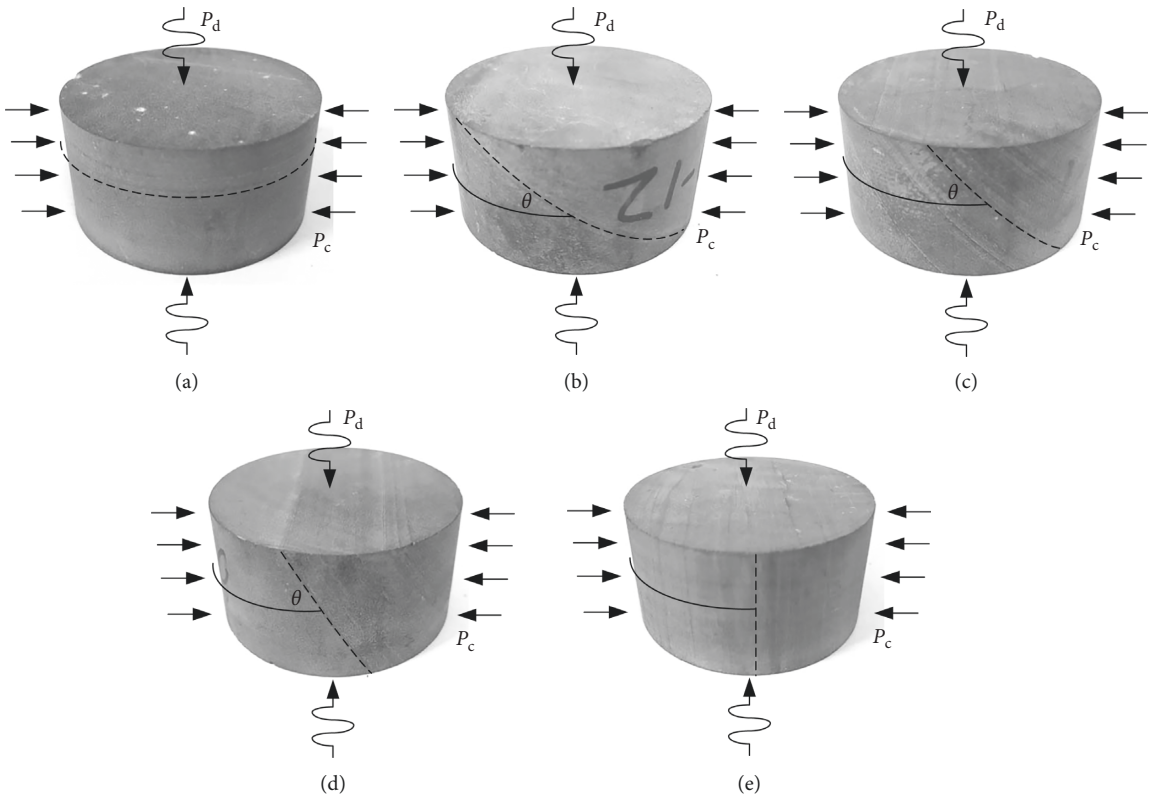

Figure 3: Five types of specimens with different dip angles (a) $\theta = 0^\circ$; (b) $\theta = 30^\circ$; (c) $\theta = 45^\circ$; (d) $\theta = 60^\circ$; (e) $\theta = 90^\circ$.

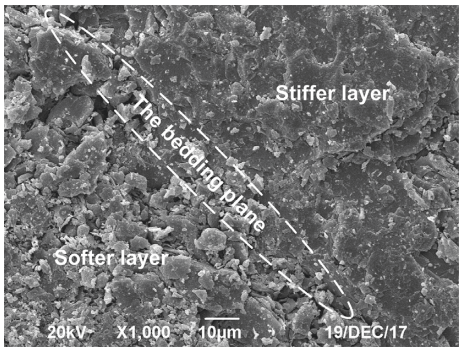

Figure 4: Microscopic structure of the slate.

Table 2: Mechanical parameters of the slate.

Mechanical parameter	θ				
	0°	30°	45°	60°	90°
E (GPa)	48.08	48.17	49.87	64.85	77.07
σ_{bc} (MPa)	167.29	79.29	73.31	66.60	147.25

4.3. Stress-Strain Behaviour. Figure 9 shows the typical stress-strain curve of the five groups of samples (0°, 30°, 45°, 60°, and 90°) subjected to three different confining pressures (0 MPa, 5 MPa, and 10 MPa). For samples in the entire groups, the plastic stage significantly increases relative to the results of the one-dimensional impact test. The stress-strain curves of the one-dimensional impact tests indicate brittle failure. By contrast, under the confining pressure condition, particularly at a relatively high level (10 MPa), the stress-strain curves present typical characteristics of elastoplastic behaviour. For example, when the value of θ is 30°, a plateau appears at the peak of the curves, indicating the samples transition from a brittle mode to a ductile mode as the confining pressure increases.

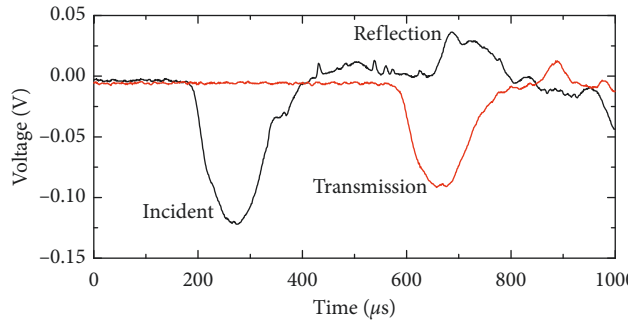

Figure 5: Experimental signals for specimen 60-1.

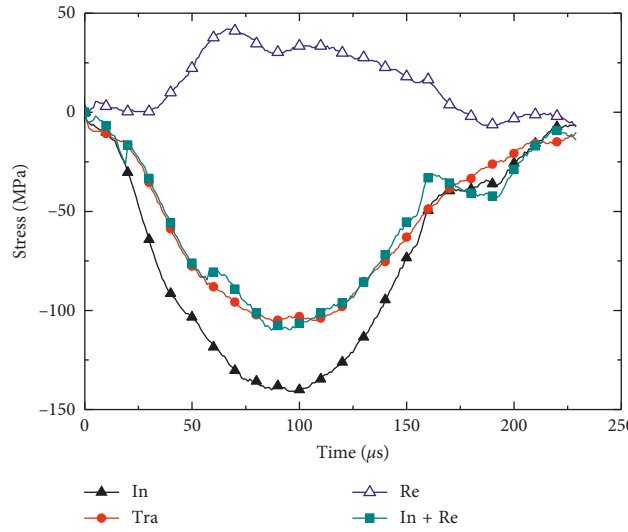

Figure 6: Stress equilibrium in specimen 60-1 (In: incident wave, Re: reflected wave, and Tr: transmitted wave).

At $\theta = 90^\circ$, the plastic stage is not easily detected when the confining pressure is 0 MPa. This result indicates that the cracks develop rapidly throughout the samples during dynamic loading. This phenomenon may result from the following two factors: (1) the impact splitting effect in one-dimensional dynamic tests and (2) the weak planes being parallel to the loading direction. Therefore, the failure patterns at $\theta = 90^\circ$ are split along the bedding plane. However, when the confining pressure increases, the plastic stage emerges again. It is clear that the confining pressure can constrain the development of cracks along the loading direction.

4.4. Influence of the Confining Pressure on the Dynamic Strength and Young's Modulus. Figure 10 shows the relationship between the dynamic strength (σ_m), Young's modulus (E), and strain rate at different confining pressures. The solid and dashed lines indicate σ_m and E, respectively.

As shown in Figure 10, the first points of the stress lines indicate the critical dynamic strength, and it is the stress least likely to cause a dynamic failure of the rock sample. The critical dynamic strength increases as the confining pressure increases. It may be because that the confining pressure is perpendicular to the loading direction and makes the samples hard to split, particularly for $\theta = 0^\circ$ and $\theta = 90^\circ$. For $30^\circ \le \theta \le 60^\circ$, the confining pressure can also increase the normal stress on the bedding plane. Thus, the friction on the bedding planes becomes larger and makes it need a higher stress to make the samples sliding failure along the bedding plane.

The strain rate effect is significant at all dip angles when the confining pressure is 5 MPa and 10 MPa. However, it differs when $\theta = 60^\circ$ and confining pressure is 0 MPa [25]. It may because the confining pressure can reduce the influence of impact splitting effect and make the failure mode of the specimen relatively simple under the medium or high loading level.

Although the rock samples were screened by a P-wave test to minimize the effect of the difference in the dynamic testing results, there is no clear tendency of Young's modulus can be detected when comparing different loading levels at one confining pressure. Lu et al. indicated that E, as one of the mechanical properties of the materials, is not sensitive to the strain rate [27].

In addition, the general trend of E is to increase with increasing confining pressure when $\theta \ge 45^\circ$. It may because the confining pressure force the microfracture in bedding planes closes at these dip angles. For $\theta = 0^\circ$ and $\theta = 30^\circ$ the

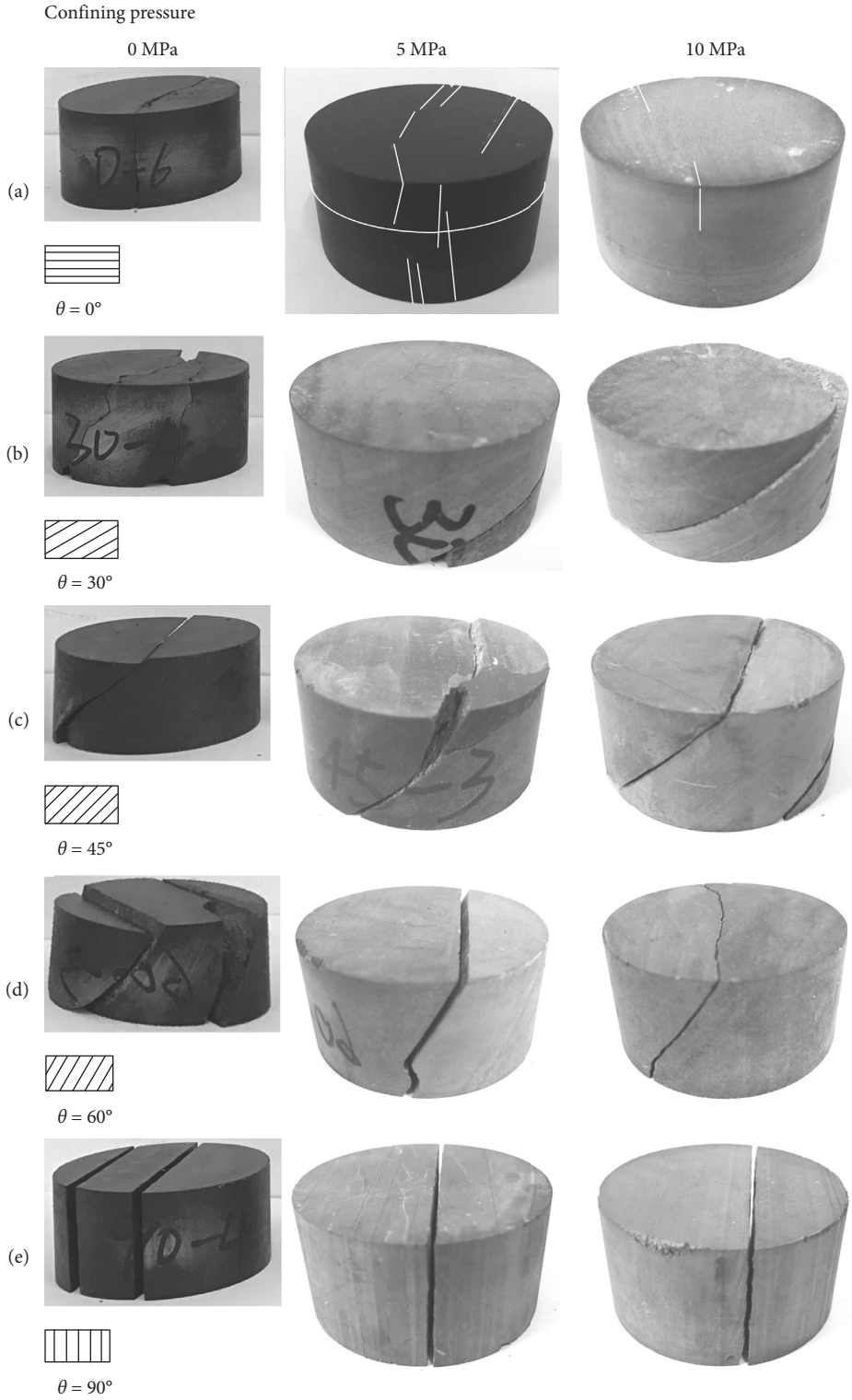

Figure 7: Recovered samples of the slate subjected to a low loading level.

direction of bedding planes and confining pressure is quite similar. The confining pressure may force the microfracture in bedding planes open. Thus, the general trend of E is to decrease with increasing confining pressure at these two angles.

5. Conclusions

The compression dynamic characteristics of the transversely isotropic rocks subjected to the confining pressure have been investigated using an improved SHPB test.

Table 3: Critical failure modes of the slate samples under different confining pressure.

θ	Confining pressure		
	0 MPa	5 MPa	10 MPa
0°	I	I	I
30°	II	III	III
45°	III	III	III
60°	III	III	III
90°	IV	IV	IV

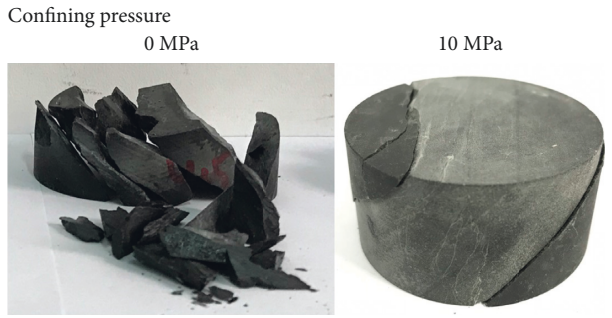

Figure 8: Recovered samples subjected to a high loading level at $\theta = 45°$.

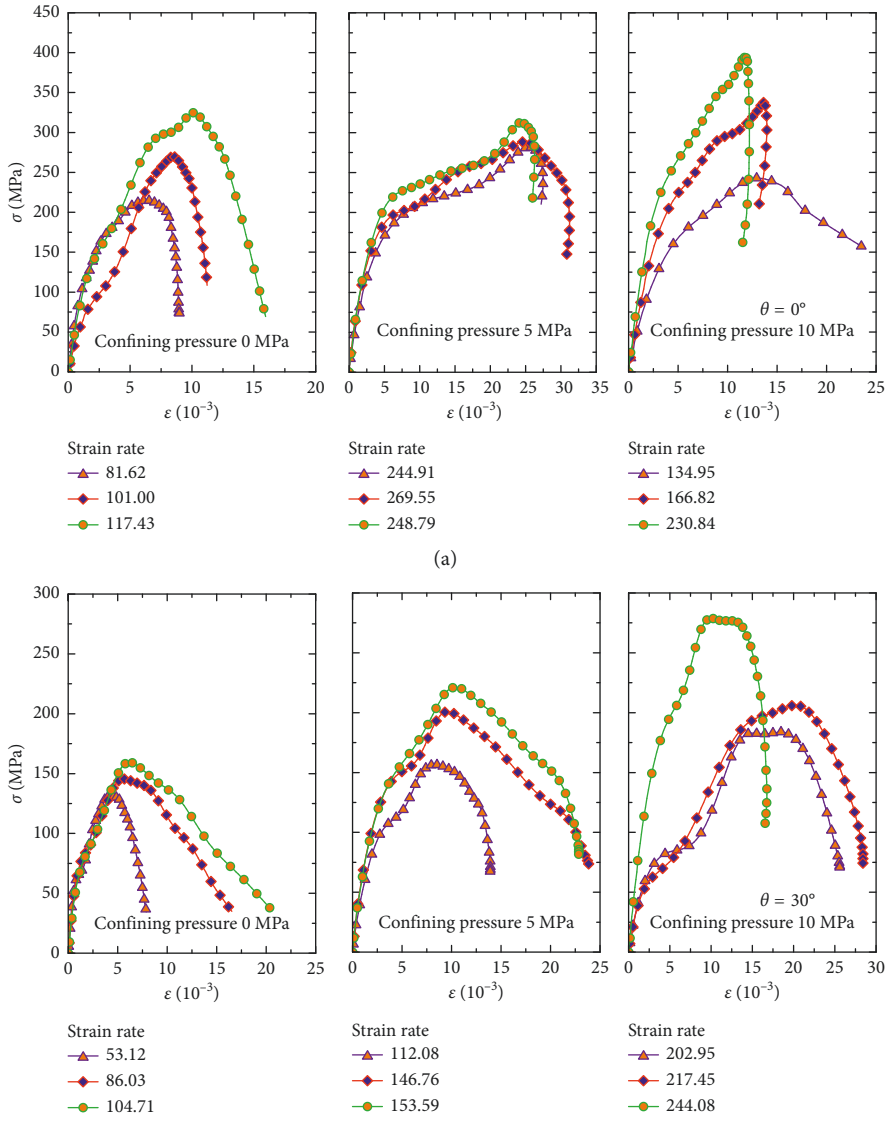

Figure 9: Continued.

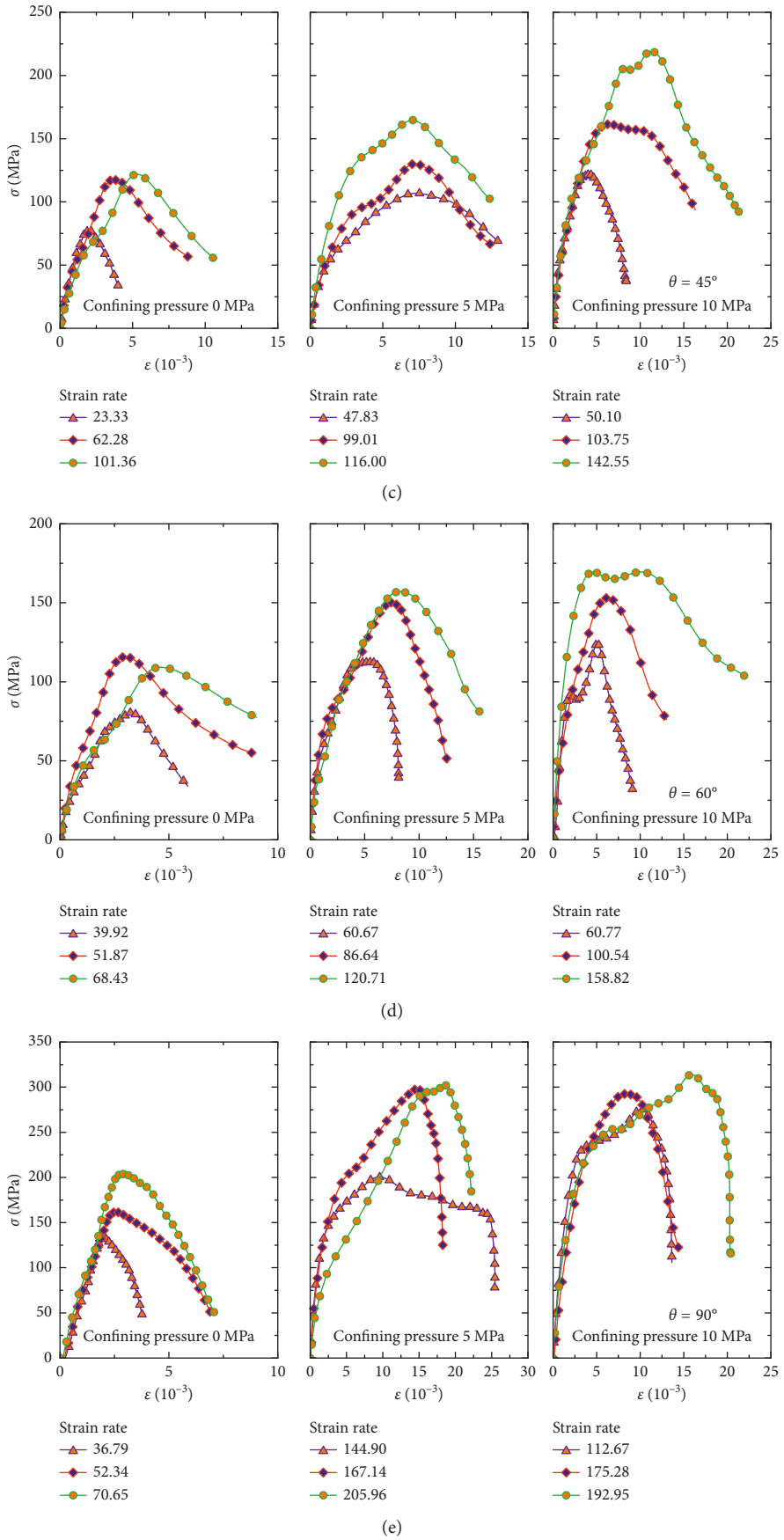

Figure 9: Stress-strain curves of samples subjected to various confining pressures and dip angles.

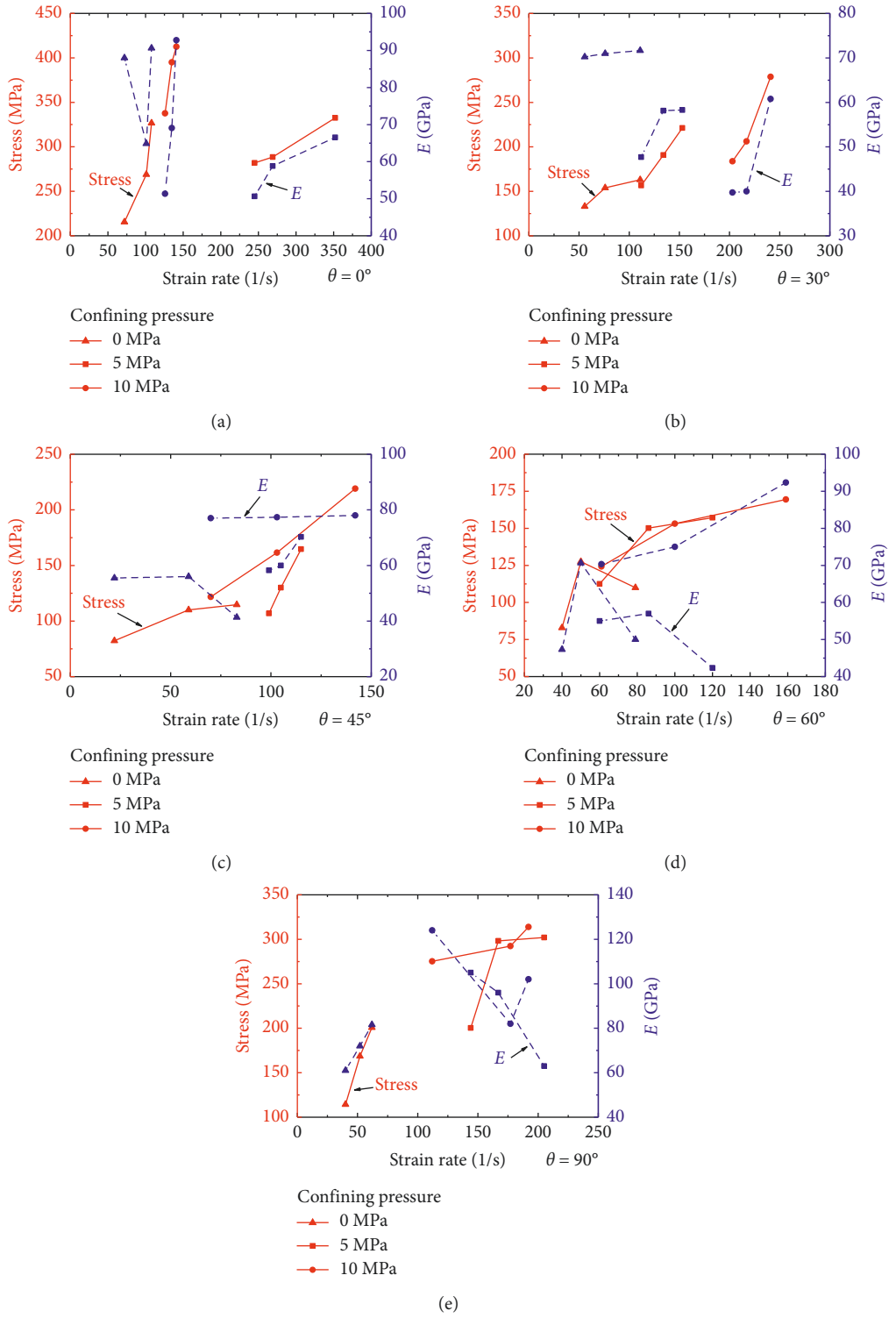

Figure 10: Strength and Young's modulus versus confining pressure.

Four main failure patterns are observed from the dynamic tests. The confining pressure can significantly constrain crack development and breakthrough. Thus, the plastic stage of the stress-strain curves is extended when the samples are subjected to confining pressure, indicating that the samples change from brittle to ductile. By constraining the cracks developed along the loading plane, confining pressure forces the samples to fail along the bedding plane.

Furthermore, confining pressure can improve the integrity and dynamic strength of the rock samples by inducing normal stress on the bedding plane. At a giving dip

angle and confining pressure, Young's modulus of the slate is not sensitive to the strain rate. However, it increases with increasing confining pressure when the dip angle $\theta \geq 45^{\circ}$ while it decreases when the dip angle $30^{\circ} \leq \theta$.

Data Availability

The experimental data used to support the findings of this study are included within the article.

Conflicts of Interest

The authors declare that they have no conflicts of interest.

Acknowledgments

The work presented in this paper was supported by the National Natural Science Foundation of China (no. 51378505 and 50808178) and the Fundamental Research Funds for the Central Universities of Central South University (no. 2017zzts161).

References

[1] A. Tavallali and A. Vervoort, "Effect of layer orientation on the failure of layered sandstone under Brazilian test conditions," *International Journal of Rock Mechanics and Mining Sciences*, vol. 47, no. 2, pp. 313–322, 2010.

[2] G. R. Adams and A. J. Jager, "Petroscopic observation of rock fracturing ahead of stope faces in deep-level gold mines," *Journal of the Southern African Institute of Mining and Metallurgy*, vol. 80, no. 6, pp. 204–209, 1980.

[3] A. Kehew, "Geology for engineers and environmental scientists," *Irish Journal of Medical Science*, vol. 182, no. 3, pp. 331–335, 1995.

[4] O. Cazacu, N. D. Cristescu, and J. F. Shao, "A new failure criterion for transversely isotropic rocks," *International Journal of Rock Mechanics and Mining Sciences*, vol. 35, no. 4-5, p. 421, 1998.

[5] E. Hoek and E. Brown, "Practical estimates of rock mass strength," *International Journal of Rock Mechanics and Mining Science & Geomechanics Abstracts*, vol. 34, no. 8, pp. 1165–1186, 1997.

[6] H. Niandou, J. Shao, J. Henry, and D. Fourmaintraux, "Laboratory investigation of the mechanical behaviour of Tournemire shale," *International Journal of Rock Mechanics and Mining Sciences*, vol. 34, no. 1, pp. 3–16, 1997.

[7] D. Q. Dan and H. Konietzky, "Numerical simulations and interpretations of Brazilian tensile tests on transversely isotropic rocks," *International Journal of Rock Mechanics and Mining Sciences*, vol. 71, no. 4, pp. 53–63, 2014.

[8] R. Nova, "The failure of transversely isotropic rocks in triaxial compression," *International Journal of Rock Mechanics and Mining Sciences & Geomechanics Abstracts*, vol. 17, no. 6, pp. 325–332, 1980.

[9] Y. M. Tien, M. C. Kuo, and C. H. Juang, "An experimental investigation of the failure mechanism of simulated transversely isotropic rocks," *International Journal of Rock Mechanics and Mining Sciences*, vol. 43, no. 8, pp. 1163–1181, 2006.

[10] F. Dai, K. Xia, J. P. Zuo, R. Zhang, and N. W. Xu, "Static and dynamic flexural strength anisotropy of barre granite," *Rock Mechanics and Rock Engineering*, vol. 46, no. 6, pp. 1589–1602, 2013.

[11] X. Liu, F. Dai, R. Zhang, and J. Liu, "Static and dynamic uniaxial compression tests on coal rock considering the bedding directivity," *Environmental Earth Sciences*, vol. 73, no. 10, pp. 5933–5949, 2015.

[12] J. Qiu, D. Li, and X. Li, "Dynamic failure of a phyllite with a low degree of metamorphism under impact Brazilian test," *International Journal of Rock Mechanics and Mining Sciences*, vol. 94, pp. 10–17, 2017.

[13] X. Li, F. Gong, J. Zhao et al., "Test study of impact failure of rock subjected to one-dimensional coupled static and dynamic loads," *Chinese Journal of Mechanical Engineering*, vol. 29, no. 2, pp. 251–260, 2010.

[14] H. Koerber, J. Xavier, and P. P. Camanho, "High strain rate characterisation of unidirectional carbon-epoxy IM7-8552 in transverse compression and in-plane shear using digital image correlation," *Mechanics of Materials*, vol. 42, no. 11, pp. 1004–1019, 2010.

[15] D. F. Malan, "Time-dependent behaviour of deep level tabular excavations in hard rock," *Rock Mechanics and Rock Engineering*, vol. 32, no. 2, pp. 123–155, 1999.

[16] R. J. Christensen, S. R. Swanson, and W. S. Brown, "Split-Hopkinson-bar tests on rock under confining pressure," *Experimental Mechanics*, vol. 12, no. 11, pp. 508–513, 1972.

[17] X. Li, Z. Zhou, T.-S. Lok, L. Hong, and T. Yin, "Innovative testing technique of rock subjected to coupled static and dynamic loads," *International Journal of Rock Mechanics and Mining Sciences*, vol. 45, no. 5, pp. 739–748, 2008.

[18] J. Zhao, H. B. Li, M. B. Wu, and T. J. Li, "Dynamic uniaxial compression tests on a granite," *International Journal of Rock Mechanics and Mining Sciences*, vol. 36, no. 2, pp. 273–277, 1999.

[19] T. C. Yet, R. Hamid, and M. Kasmuri, "Dynamic stress-strain behaviour of steel fiber reinforced high-performance concrete with fly ash," *Advances in Civil Engineering*, vol. 2012, Article ID 907431, 6 pages, 2012.

[20] Q. B. Zhang and J. Zhao, "Determination of mechanical properties and full-field strain measurements of rock material under dynamic loads," *International Journal of Rock Mechanics and Mining Sciences*, vol. 60, no. 8, pp. 423–439, 2013.

[21] F.-Q. Gong and G.-F. Zhao, "Dynamic indirect tensile strength of sandstone under different loading rates," *Rock Mechanics and Rock Engineering*, vol. 47, no. 6, pp. 2271–2278, 2014.

[22] Y. Zhao, G.-F. Zhao, Y. Jiang, D. Elsworth, and Y. Huang, "Effects of bedding on the dynamic indirect tensile strength of coal: laboratory experiments and numerical simulation," *International Journal of Coal Geology*, vol. 132, pp. 81–93, 2014.

[23] X. B. Li, T. S. Lok, J. Zhao, and P. J. Zhao, "Oscillation elimination in the Hopkinson bar apparatus and resultant complete dynamic stress-strain curves for rocks," *International Journal of Rock Mechanics and Mining Sciences*, vol. 37, no. 7, pp. 1055–1060, 2000.

[24] X. B. Li, T. S. Lok, and J. Zhao, "Dynamic characteristics of granite subjected to intermediate loading rate," *Rock Mechanics and Rock Engineering*, vol. 38, no. 1, pp. 21–39, 2005.

[25] H. Kolsky, "Stress waves in solids," *Journal of Sound and Vibration*, vol. 1, no. 1, pp. 88–110, 1964.

[26] X. Zhang, X. Ou, F. Gong, and J. Yang, "Effects of bedding on the dynamic compressive properties of low anisotropy slate," *Rock Mechanics and Rock Engineering*, pp. 1–10, 2018.

[27] X. Lu, J. Xu, H. Ge et al., "Effects of confining pressure on mechanical behaviors of sandstone under dynamic impact loads," *Chinese Journal of Rock Mechanics and Engineering*, vol. 29, no. 1, pp. 193–201, 2010.